Heating *N*-methylanthranilic acid (**87**) with thionyl chloride gave an unstable sulfinamide anhydride (**86**), which was treated with 3,4-dihydro-β-carboline (**60**) in dry benzene at room temperature to afford regioselectively evodiamine (**84**), in 65% yield. In this reaction, the sulfinamide anhydride **86** was converted into the iminoketene **85**, which reacted regioselectively with 3,4-dihydro-β-carboline (**60**) by cycloaddition pattern to form evoidamine.[30]

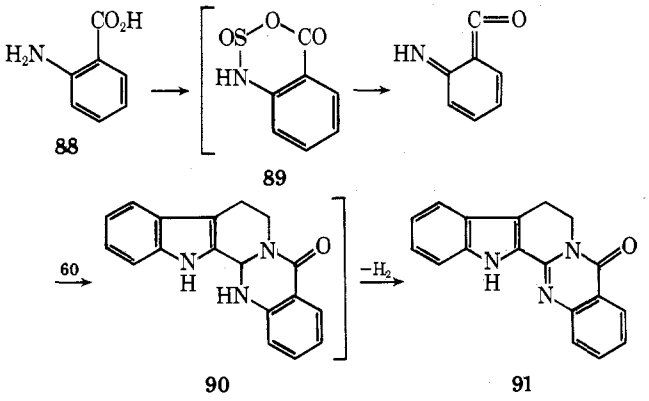

(30) T. Kametani, T. Higa, K. Fukumoto, and M. Koizumi, *Heterocycles*, **4**, 23 (1976).

Rutecarpine (**91**) is also obtained in one step by the same way; thus a treatment of the sulfinamide anhydride **89**, derived from anthranilic acid (**88**), with **60** gave, in 85% yield, rutecarpine (**91**), by a spontaneous dehydrogenation of the firstly formed product (**90**).[30]

Thus, one-step syntheses for evodiamine and rutecarpine have been accomplished by retro mass spectral methods.

In this Account, we have shown retro mass spectral analysis to provide a simple and effective synthetic approach to natural products having a complicated structure. Most of the important types of fragmentation in the mass spectrum are summarized as: (1) simple carbon–carbon bond cleavages; (2) cleavages involving heteroatoms; (3) retro-Diels–Alder types of concerted cleavages; and (4) rearrangements. We have discussed the power and generality of our method to syntheses of natural products which show fragmentation processes of types 1 and 3. Unfortunately, we have no successful results in retro mass spectral synthesis due to type 4 fragmentation. We have also found a new reaction of iminoketenes, generated in situ from anthranilic acids, with the imine system and have developed several new synthetic methods for some isoquinoline and indole alkaloids. We believe that retro mass spectral synthesis can be extended to the synthesis of tetracyclins, terpenes, and steroidal hormones in the future.

Nuclear Reactions Revisited with Very Heavy Ions

John R. Huizenga

Department of Chemistry and Nuclear Structure Research Laboratory, University of Rochester, Rochester, New York 14627

Received February 2, 1976

Intense excitement has been generated during the last decade by nuclear theorists who have predicted islands or regions of enhanced nuclear stability[1] for elements with Z values considerably larger than those now known (e.g., atomic numbers $Z = 110$ to 126). The calculations leading to the predicted properties of superheavy nuclei are based in part on experimental information about shape-dependent nuclear shells which account for the recently discovered two-humped fission barriers.[2] Although some effort has gone into various experimental searches for these new elements, no evidence for them has been found to date.[1] Reactions with heavy ions are possibly one mode of producing the superheavy elements and, hence, the development of heavy-ion science has been rapidly accelerated.

The search for superheavy elements was also one of the initial motivations for my interest in the various types of mechanisms involved in the interaction between two large complex nuclei. However, these reaction mechanisms are of great fundamental interest in themselves. In this Account I discuss the mechanisms of reactions between very heavy ions, with emphasis on the recently discovered strongly damped collision process. This new process has now been reported for reactions induced with heavy-ion projectiles from nitrogen to xenon.[3-21] In order to place this new reaction process

John R. Huizenga received his B.A. degree from Calvin College, and the Ph.D. from the University of Illinois (in 1949). He was employed at the Argonne National Laboratory until 1967 when he joined the University of Rochester as Professor of Chemistry and Physics. His research interests are in nuclear chemistry and in particular in nuclear reactions and fission. Professor Huizenga is the 1975 recipient of the ACS Award for Nuclear Applications in Chemistry, and this Account is based in part on his award address.

(1) For reviews of this subject and references, see *Phys. Scr.*, **10A**, 1 (1974); G. N. Flerov, "Reactions between Complex Nuclei", Vol. 2, North-Holland Publishing Co., Amsterdam, 1974, p 459.

(2) For references in this area, see R. Vandenbosch and J. R. Huizenga, "Nuclear Fission", Academic Press, New York, N.Y., 1973.

(3) A. G. Artukh, G. F. Gridnev, V. L. Mikheev, V. V. Volkov, and J. Wilczyński, *Nucl. Phys. A*, **211**, 299 (1973); **215**, 91 (1973).

(4) F. Hanappe, M. Lefort, C. Ngo, J. Peter, and B. Tamain, *Phys. Rev. Lett.*, **32**, 738 (1974).

(5) K. L. Wolf, J. P. Unik, J. R. Huizenga, J. R. Birkelund, H. Freiesleben, and V. E. Viola, *Phys. Rev. Lett.*, **33**, 1105 (1974).

(6) J. V. Kratz, A. E. Norris, and G. T. Seaborg, *Phys. Rev. Lett.*, **33**, 502 (1974).

(7) S. G. Thompson, L. G. Moretto, R. C. Jared, R. P. Babinet, J. G. Galin, M. M. Fowler, R. C. Gatti, and J. B. Hunter, *Phys. Scr.*, **10A**, 36 (1974).

(8) J. Péter, C. Ngô, and B. Tamain, *J. Phys. Lett.*, **36**, L23 (1975).

(9) J. C. Jacmart, P. Colombani, H. Doubre, N. Frascaris, N. Poffe, M. Riou, J. C. Roynette, C. Stéphan, and A. Weidinger, *Nucl. Phys. A*, **242**, 175 (1975).

(10) P. Colombani, N. Frascaria, J. C. Jacmart, M. Riou, C. Stéphan, H. Doubre, N. Poffé, and J. C. Roynette, *Phys. Lett. B*, **55**, 45 (1975).

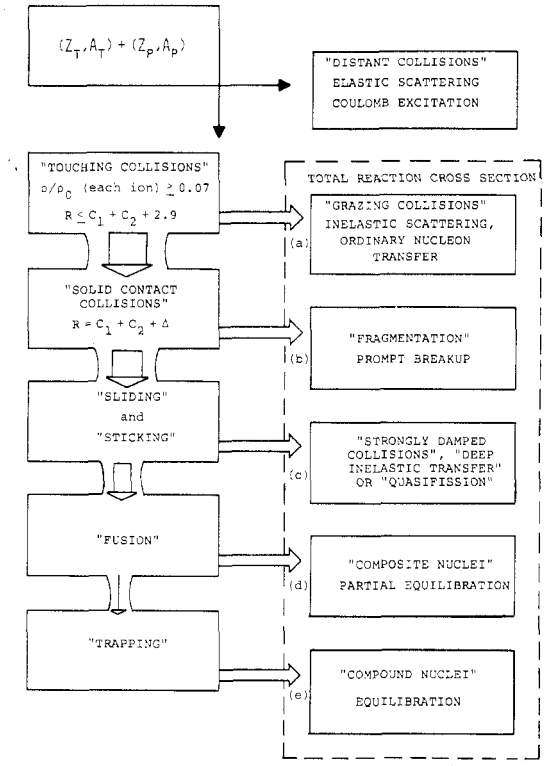

Figure 1. Schematic classification of heavy-ion reactions.

in perspective, an overall classification of heavy-ion nuclear reactions, similar to that of Swiatecki,[22] is proposed in Figure 1.

The various terms in Figure 1 such as "distant" and "touching" collisions are to be understood in the context of a matter density of nuclei with diffuse surfaces. The radial dependence of the nuclear density ρ is approximated by a two-parameter Fermi distribution function,

$$\rho = \rho_0/\{1 + \exp[(r - C)/a]\} \qquad (1)$$

where C is the nuclear half-density radius, a is a measure of the surface diffuseness, and ρ_0 is the central density. *Distant collisions* occur when the extreme tails of the nuclear density of each nucleus overlap, where the centers of the nuclei are separated by a distance greater than $C_1 + C_2 + 2.9$ fm (the origin of this distance is discussed later). At these large distances only electromagnetic interactions, slightly modified by the tail of the nuclear potential, occur. *Touching collisions* take place at nuclear separation distances equal to or less than $C_1 + C_2 + 2.9$ fm. At this distance the nuclear density of each nucleus corresponds to about 7% of its central density. The touching collisions lead to nuclear interaction and are responsible for the total reaction cross section.

The flux from touching collisions is subdivided into five different types of reaction products in Figure 1. Two complex nuclei which touch but do not make *solid contact* produce a *grazing collision.* Solid contact is defined by a distance equal to or slightly larger than the sum of the half-density radius of each ion, a distance which is approximated by $C_1 + C_2 + \Delta$. A solid contact collision where the nuclei do not *slide on each other or stick* produces *fragmentation.* Nuclei which stick or slide on each other but do not *fuse* can be viewed in terms of a binary complex which on breakup leads to the recently discovered strongly damped collisions (*deep-inelastic transfer* or *quasifission*). *Fusion* implies the loss of identity of projectile and target. Nuclei which fuse but are not trapped in a potential-energy pocket form a *composite nucleus* where only partial equilibrium is attained before decay. The remaining nuclei are *trapped,* giving a *compound nucleus* with equilibration of all degrees of freedom. The above reaction types do not have sharp boundaries, but overlap to some degree. For example, at some angles the energies of the grazing and strongly damped collisions flow continuously into each other, and some fraction of the strongly damped collisions has large amounts of mass transfer similar to the reaction products following fusion.

The touching collisions for light-ion reactions at low and medium energy undergo both grazing collisions (larger impact parameters) and solid-contact collisions which have a high probability for fusion. A large fraction of the fusion events lead to trapping and compound nucleus formation, although some fraction of the fusion events forms a composite system (preequilibrium decay). The lifetimes of the various reactions in Figure 1 increase in the direction of flow and produce very different reaction products with characteristic properties such as energy and angular distribution. The first evidence for a new process for very heavy ion reactions was obtained from a study of ^{40}Ar-induced reactions of ^{232}Th, where a sizable yield of reaction products, highly damped in kinetic energy but with masses near the projectile, was observed.[3] For ^{84}Kr- and ^{136}Xe-induced reactions on heavy targets, the strongly damped collisions represent by far the dominant reaction[4-6,16,19] and no evidence has been found for the compound nucleus process (upper limits of 2 to 10% of the total reaction cross section are established).[23,24]

The characteristic features of this new reaction mechanism for heavy ions are: (1) strong damping of the initial relative kinetic energy of the target and projectile nuclei into internal excitation energy, resulting in a range of binary-product kinetic energies down to the Coulomb energies for charge centers of highly deformed fragments; (2) considerable nucleon transfer taking place during the short lifetime of the intermediate, slightly overlapping double-nucleus complex (however, the reaction product masses are distributed into two groups, with average masses near those of the target and

(11) J. Wilczyński, K. Swiek-Wilczynska, J. S. Larsen, J. C. Acquadro, and P. R. Christensen, *Nucl. Phys. A,* **244,** 147 (1975).
(12) R. Albrecht, W. Dünnweber, G. Graw, H. Ho, S. G. Steadman, and J. P. Wurm, *Phys. Rev. Lett.,* **34,** 1400 (1975).
(13) T. M. Cormier, A. J. Lazzarini, M. A. Newhausen, A. Sperduto, K. Van Bibber, F. Videbaek, G. Young, E. B. Blum, L. Herreid, and W. Thoms, *Phys. Rev.* [*Sect.*] C **13,** 682 (1976).
(14) L. G. Moretto, S. S. Kataria, R. C. Jared, R. Schmitt, and S. G. Thompson, *Nucl. Phys. A,* **255,** 491 (1975).
(15) R. Babinet, L. G. Moretto, J. Galin, R. Jared, J. Moulton, and S. G. Thompson, *Nucl. Phys. A,* **258,** 172 (1976).
(16) R. Vandenbosch, M. P. Webb, and T. D. Thomas, *Phys. Rev. Lett.,* **36,** 459 (1976).
(17) J. Galin, L. G. Moretto, R. Babinet, R. Schmitt, R. Jared, and S. G. Thompson, *Nucl. Phys. A,* **255,** 472 (1975).
(18) L. G. Moretto, J. Galin, R. Babinet, Z. Fraenkel, R. Schmitt, R. Jared, and S. G. Thompson, *Nucl. Phys. A,* **259,** 173 (1976).
(19) W. U. Schröder, J. R. Birkelund, J. R. Huizenga, K. L. Wolf, J. P. Unik, and V. E. Viola, *Phys. Rev. Lett.,* **36,** 514 (1976).
(20) H. C. Britt, B. H. Erkilla, R. H. Stokes, H. H. Gutbrod, F. Plasil, R. L. Ferguson, and M. Blann, *Phys. Rev.* [*Sect.*] C, 13, 1483 (1976).
(21) B. Tamain, F. Plasil, C. Ngô, J. Péter, M. Berlanger, and F. Hanappe, *Phys. Rev. Lett.,* **36,** 18 (1976).
(22) W. Swiatecki, Lawrence Berkeley Laboratory preprint LBL-4296 (1975).
(23) J. Péter, C. Ngô, and B. Tamain, *Nucl. Phys. A,* **250,** 351 (1975).
(24) K. L. Wolf, J. P. Unik, J. R. Huizenga, J. R. Birkelund, H. Freiesleben, W. U. Schröder, and V. E. Viola, unpublished results, 1975.

projectile; the product masses and charges are correlated with the kinetic energy dissipated); (3) forward-peaked angular distributions observed for the products with masses near the projectile mass with features characteristic of a fast peripheral or direct reaction occurring on a time scale of 10^{-21} sec or less (for the heaviest projectile-target combinations, the differential cross sections for products near the projectile mass are strongly peaked at angles slightly forward of $\theta_{1/4}$ (the angle where the elastic-to-Rutherford cross section ratio is 0.25)).

The fragmentation process is included in Figure 1 for completeness. Some evidence exists for this process at very high energies; however, it is unimportant at projectile energies of ≤10 MeV/nucleon and will not be further considered here.

The reaction process leading to composite nuclei appears to be of importance for heavy-ion reactions, but for lack of space will be mentioned only in this introductory section. Heavy-ion reactions are unique in that extremely large orbital angular momenta are involved in such collisions (l waves up to 500$\hbar$ for 1130-MeV ^{136}Xe + ^{209}Bi). Calculations with a charged liquid drop model[25] predict that no nucleus can support more than a limiting angular momentum of about 100$\hbar$. The nuclei stable with such large angular momenta occur near $A \approx 130$, and as A increases, instability sets in at decreasing values of l. When these limiting angular momenta are exceeded, the fission barrier vanishes, resulting in nuclear instability. This type of reaction process is expected to be fast enough so that only partial equilibration of the various degrees of freedom occurs. Although there is no definitive experimental evidence for this mechanism at present, indirect evidence for it is provided by fission studies, e.g., from ^{40}Ar-induced fission of heavy targets.[26] Careful measurements of the angular distribution of fission fragments can, in principle, separate this "zero barrier" type fission from compound-nucleus fission.

The Potential and Elastic Scattering

In the absence of an attractive nuclear potential, the distance of closest approach between two heavy ions as a function of scattering angle is given by[27]

$$D(\theta) = \frac{Z_1 Z_2 e^2}{2E_{cm}}\left(1 + \operatorname{cosec}\frac{1}{2}\theta\right) = \eta\lambda\left(1 + \operatorname{cosec}\frac{1}{2}\theta\right) \quad (2)$$

where λ and η are, respectively, the reduced wavelength and Sommerfeld parameter ($Z_1 Z_2 e^2/\hbar v$) at infinite ion separation (for large η, $[D(\theta)/\lambda] \gg 1$). For large values of $D(\theta)$ (or small values of θ), the scattering is dominated by the Coulomb potential. At smaller separation distances, the Coulomb field is modified by the nuclear interaction leading to the onset of grazing collisions.

Information about the ion–ion nuclear potential is obtained through studies of the elastic scattering and inelastic reaction cross sections. An example of an elastic scattering angular distribution is given in Figure 2A for scattering of 712-MeV ^{84}Kr on ^{209}Bi.[28] A theoretical

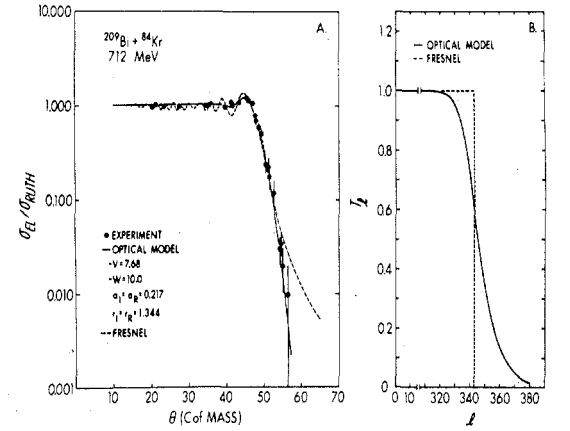

Figure 2. (A) Elastic scattering angular distribution.[28] (B) Transmission coefficients as a function of angular momentum for the reaction in (A).

optical model fit to these data is shown also in Figure 2A. The basic assumption of this quantum-mechanical model is that the scattering is describable by a simple, complex potential which depends only upon the separation r of the centers of mass of the two heavy ions. Frequently, the nuclear potential is assumed to have a Saxon–Woods form, $f(r) = \{1 + \exp[(r - R)/a]\}^{-1}$, so that the radial dependence of the total potential is given by

$$V(l,r) = V_C(r) + V_l(r) + V_N f_R(r) + iW_N f_I(r) \quad (3)$$

where the terms are the Coulomb, centrifugal, and nuclear potentials, respectively, and $R = r_{opt}(A_p^{1/3} + A_T^{1/3})$. The diffuseness parameters a and radial parameters r_{opt} may be the same or different for the real (V_N) and imaginary (W_N) parts of the nuclear potential. Such a parametrization of the optical potential is subject to considerable ambiguities when applied to the scattering of strongly absorbed particles such as heavy ions.[29,30] This leads to a wide choice of potentials, each of which gives a good fit to the elastic scattering data. One such four-parameter optical model which fits the ^{209}Bi + ^{84}Kr (712 MeV) elastic scattering data[28] is described by the values of V, W, $a_I = a_R$, and $r_I = r_R$ given in Figure 2A. Various sets of real potentials which give equivalent fits to the elastic scattering data tend to give a common value of the real potential at the strong absorption radius. The strong absorption radius for the optical model[31] is defined by

$$R_{SA}/\lambda = \eta + [\eta^2 + l_{1/2}(l_{1/2} + 1)]^{1/2} \quad (4)$$

where R_{SA} represents the distance of closest approach for the classical Rutherford orbit of angular momentum l for which the transmission coefficient $T_l = 0.5$. (Inclusion of the nuclear potential reduces R_{SA} by 0.05 fm for the reaction in Figure 2a.)

The transmission coefficients T_l for the optical potential used to fit the elastic scattering of 712-MeV ^{84}Kr

(25) S. Cohen, F. Plasil and W. J. Swiatecki, *Ann. Phys. (N.Y.)*, **82**, 557 (1974).
(26) J. R. Huizenga, *Nukleonika*, **20**, 291 (1975).
(27) P. R. Christensen, V. I. Manko, F. D. Becchetti, and R. J. Nickles, *Nucl. Phys. A*, **207**, 33 (1973).
(28) J. R. Birkelund, J. R. Huizenga, H. Freiesleben, K. L. Wolf, J. P. Unik, and V. E. Viola, Jr., *Phys. Rev.* [*Sect.*] *C*, **13**, 133 (1976).
(29) J. S. Blair, "Proceedings of the Conference on Nuclear Reactions Induced by Heavy Ions", W. Hering and R. Bock, Ed., North-Holland Publishing Co., Amsterdam, 1970; G. R. Satchler, "Reactions between Complex Nuclei", Vol. 2, North-Holland Publishing Co., Amsterdam, 1974, p 171.
(30) J. B. Ball, C. B. Fulmer, E. E. Gross, M. L. Halbert, D. C. Hensley, C. A. Ludemann, M. J. Saltmarsh, and G. R. Satchler, *Nucl. Phys. A*, **252**, 208 (1975).
(31) J. S. Blair, Lectures in Theoretical Physics, Vol. 8, University of Colorado, Boulder, Colo., 1966; B. Fernandez and J. S. Blair, *Phys. Rev.* [*Sect.*] *C*, **1**, 523 (1970).

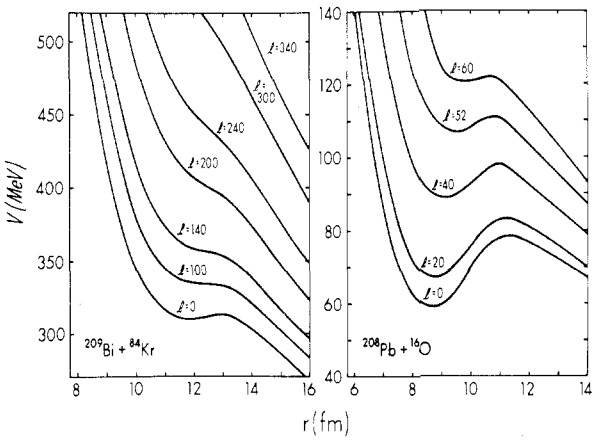

Figure 3. Total real potentials based on the nuclear proximity potential.[22]

on ^{209}Bi are plotted in Figure 2B. The value of T_l falls from 0.9 to 0.1 between l values of 333 and 362.

As mentioned above, elastic scattering measurements determine the real potential at the strong absorption radius R_{SA}. In addition, some information on the slope of the real potential near R_{SA} is obtained by studying the energy dependence[32] of elastic scattering (while this technique is useful for light-ion reactions, it is probably not very useful for heavy-ion reactions due to their strong absorption near the nuclear surface). Essentially nothing is learned about the nuclear potential from heavy-ion elastic scattering at radial distances smaller than R_{SA}. Hence, one must resort to models in order to estimate the radial dependence of the nuclear potential. These trial potentials are then tested for different types of reactions which are sensitive to the potential at smaller radii. One model[26,28] assumes a Saxon–Woods form of the nuclear potential at distances between $C_1 + C_2$ and R_{SA} and evaluates the Saxon–Woods parameters from the liquid-drop maximum force at $C_1 + C_2$ and the value of the potential from elastic scattering at R_{SA}. In addition, two theoretical potentials, the proximity potential[22,33] and the energy-density potential,[34] have been proposed for calculating the interaction energy between two colliding ions. At small values of r, where the nuclear densities pile up, both of these theoretical nuclear potentials rise rapidly. This repulsion develops both because of the exclusion principle and because the nucleon–nucleon force saturates at the normal nuclear density.

In Figure 3, the radial dependence of the effective total real potential $V = V_C + V_l + V_N$ is plotted for the $^{209}Bi + ^{84}Kr$ and $^{208}Pb + ^{16}O$ reactions (where V_N is approximated by the proximity potential). The most important feature displayed in this figure is the presence of deep minima or pockets in the total potentials for the $^{208}Pb + ^{16}O$ reaction and the absence of deep minima for the $^{209}Bi + ^{84}Kr$ reaction. For reactions with pockets, there is a sharp discontinuity in the distance of closest approach, or penetration depth as a function of l. This discontinuity occurs for the l wave whose potential barrier height equals $E_{c.m.}$.[35] For the $^{208}Pb + ^{16}O$ reaction at a center-of-mass energy of 100 MeV, this discontinuity in penetration depth occurs for $l = 42\hbar$, a value of l somewhat smaller than $l_{max} = 52\hbar$ calculated on the basis of an interaction radius of 12.5 fm.[30] For the $^{209}Bi + ^{84}Kr$ reaction, where the Coulomb potential is so large that the nuclear potential is unable to produce pockets, the distance of closest approach decreases with l but has *no* discontinuity. In both of these cases there is a band of orbits which experiences the attractive nuclear potential without plunging into the interior region of the nucleus. This feature of heavy-ion reactions gives credence to the postulate that the maximum angular momentum is determined by the imaginary potential and *not* the real potential. Some evidence for the sensitivity of elastic scattering of ^{84}Kr on ^{209}Bi to the imaginary-potential geometry has been observed.[28]

Interaction Radii and Total Reaction Cross Sections

The experimental total reaction cross section is obtained by summing all the reaction channels initiated by "touching collisions" (see Figure 1). This is usually impractical for heavy-ion reactions, where a large number of inelastic channels are open. Therefore, the total reaction cross section is often calculated from an optical-model analysis of the elastic-scattering angular distribution, where

$$\sigma_R(\text{optical}) = \pi\lambda\!\!\!^{-2} \sum_l (2l + 1)T_l \qquad (5)$$

Insofar that a large number of angular-momentum waves contribute to the heavy-ion total reaction cross section, a much simpler classical model gives a reliable estimate of the total reaction cross section. Frahn[36] has shown that the elastic-scattering angular distributions are approximately reproduced by an expression in which all partial waves with $l \leq l_{max}$ are absorbed ($T_l = 1$) and all partial waves $l > l_{max}$ are elastically scattered ($T_l = 0$). In this model, the maximum angular momentum, the interaction radius, and the total reaction cross section, respectively, are given by

$$l_{max} = \eta \cot(\theta_{1/4}/2) \qquad (6)$$

$$R_{INT} = \eta\lambda\!\!\!^{-}[1 + \text{cosec}(\theta_{1/4}/2)] \qquad (7)$$

$$\sigma_R(\text{Fresnel}) = \pi\lambda\!\!\!^{-2}(l_{max} + 1)^2 \qquad (8)$$

where $\theta_{1/4}$ is the "quarter point" angle obtained from the experimental elastic scattering angular distribution as the angle for which $\sigma_{el}/\sigma_{Ru} = 0.25$. A comparison of the Fresnel model predictions and the experimental data[28] for the elastic scattering of 712-MeV ^{84}Kr on ^{209}Bi is shown in Figure 2A. The transmission coefficients for the Fresnel and optical models are compared in Figure 2B. Due to its simplicity, the Fresnel model is extremely useful for estimating the total reaction cross section between two heavy ions. The procedure is as follows: (a) calculate the interaction radius from eq 9, (b) calculate the "quarter point" from eq 7, (c) calculate the value of l_{max} from eq 6, and, finally, (d) calculate the total reaction cross section from eq 8. The Fresnel and optical models lead to nearly the same results. This is illustrated by a comparison of several relevant quantities in Table I for the reactions between a

(32) D. A. Goldberg and S. M. Smith, *Phys. Rev. Lett.*, **33**, 715 (1974).
(33) J. Randrup, W. J. Swiatecki, and C. F. Tsang, Lawrence Berkeley Laboratory preprint LBL-3603 (1974).
(34) C. Ngô, B. Tamain, J. Galin, M. Beiner, and R. J. Lombard, *Nucl. Phys. A*, **240**, 353 (1975), C. Ngô, B. Tamain, M. Beiner, R. J. Lombard, D. Mas, and H. H. Deubler, *ibid.*, **252**, 237 (1975).
(35) N. K. Glendenning, *Rev. Mod. Phys.*, **47**, 659 (1975).
(36) W. E. Frahn, *Phys. Rev. Lett.*, **26**, 568 (1971); *Ann. Phys. (N.Y.)*, **72**, 524 (1972).

^{209}Bi target and ^{40}Ar, ^{84}Kr, and ^{136}Xe projectiles.[19,28] The reaction cross sections deduced from the two models for the above reactions agree to within about 3%.

The Fresnel interaction radius R_{INT} (see eq 7) and the optical model strong-absorption radius R_{SA} (see eq 4) have been compared for a large number of heavy-ion reactions and found to be nearly the same.[28] This is not surprising in that both radii represent the same classical distance of closest approach, where l_{max} in the Fresnel model is approximately equal to $l_{1/2}$ in the optical model. (Inclusion of the nuclear potential introduces a negligible correction for very heavy ion reactions.) This interaction radius is associated with touching collisions and is the distance responsible for the total reaction cross section.

If this interaction radius is parameterized by $r_0(A_P^{1/3} + A_T^{1/3})$, the value of r_0 decreases with the product A_1A_2. This dependence is due to the diffuseness of the nuclear surface which is a smaller fraction of the interaction radius as A_1A_2 increases. The experimental interaction or strong absorption radii for a large number of heavy-ion reactions are well reproduced by the simple expression[28]

$$R_{INT} = C_p + C_T + S \qquad (9)$$

where C_p and C_T are the projectile and target half-density matter radii[37,38] of a two-parameter Fermi distribution (see eq 1) and S is a constant equal to 2.9 ± 0.3 fm. If the diffuseness parameter a in eq 1 is assumed to be 0.55 fm, the interaction radius corresponds to a density of about 7 ± 2% of the central density of each nucleus in the overlap region. If the "equivalent sharp radius" [28] is introduced into eq 9, where this radius is given by the approximate expression $R = (1.13 + 0.0002A)A^{1/3}$, then a reasonable fit to the experimental interaction radii is obtained with a constant of 2.5 fm. The value of C in eq 9 is related to R by $C = (1 - R^{-2})R$, which assumes the diffuseness parameter a in eq 1 to be 0.551 fm.

Experimental Features of the New Strongly Damped Collision Process

Previously we discussed potentials with and without pockets. The first type of potential is applicable for relatively light projectiles where the energy is in the range between one and two times the Coulomb barrier. In such cases the center-of-mass energy intersects a pocket in the effective potential, and a sharp discontinuity occurs in $D(l)$. Touching collisions for light ions are known to have a high probability for "trapping" with subsequent compound nucleus formation (see Figure 1). If all the degrees of freedom are frozen except the separation between the ions, a necessary condition for compound nucleus formation is that the one-dimensional total potential energy have a pocket and that sufficient dissipative forces exist to reduce the kinetic energy so that the projectile is trapped. In addition, the dynamical trajectory for fusing the system must pass inside the fission saddle point in a multidimensional space.[39]

The second type of effective potential is applicable for the heavier ion reactions. The Coulomb force for these large charges is so overwhelming that pockets in the potential energy curves occur for few, if any, angular-momentum waves.[26,40,41] As a consequence, when heavy targets are bombarded with heavy projectiles, e.g., argon, copper, krypton, and xenon, at moderate energies (<10 MeV/nucleon), a major fraction of the total reaction cross section goes into a new reaction process[3-10,16-20] yielding reaction products with characteristics completely different from fusion products. Although small cross sections of a similar process[11-15] with large energy damping have been reported for reactions between "lighter" heavy ions at energies considerably above the Coulomb barrier, only very heavy ion reactions are considered here.

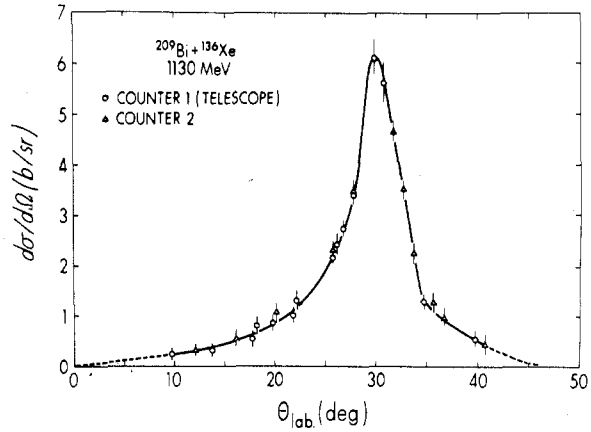

Figure 4. Differential reaction cross section in barn/sr as a function of laboratory angle.[19]

Angular Distributions. The angular distribution of the group of reaction products with average masses near ^{136}Xe observed for the ^{209}Bi + ^{136}Xe reaction[19] at 1130 MeV is shown in Figure 4. Such an angular distribution is characteristic of those observed for reactions between two very complex nuclei, and is evidence for a nonequilibrium process occurring on a relatively fast time scale. Transformation of this angular distribution into the center-of-mass system requires knowledge of the product masses. However, the products at the peak angle are very near the projectile mass and lead to a center-of-mass angle near the elastic scattering quarter point of $\theta_{1/4}^{cm} = 54°$.

Integration of the angular distribution in Figure 4 gives a cross section of 2840 ± 150 mbarns, in close agreement with the optical model total reaction cross section of 2780 ± 100 mbarns (see Table I). Hence, there is no evidence for any of the l waves giving a "compound nucleus" (the limit on the number of l waves which could lead to a "compound nucleus" is not well determined, since the first 100l waves gives a cross section of only 118 mbarns).

As the projectile energy is increased for the ^{209}Bi + ^{84}Kr reaction, the angle corresponding to the peak cross section moves to smaller angles. At the largest energy there is some evidence that the differential reaction cross section at angles near 0° is composed of contributions from both positive and negative angles. The first evidence for negative-angle contributions to the reaction cross section was reported for the ^{232}Th + ^{40}Ar reaction at bombarding energies of 288 and 379 MeV.[3,42] The

(37) C. W. Jager, H. deVries, and C. deVries, *At. Nucl. Data Tables*, **14**, 479 (1974).
(38) W. D. Myers, *Nucl. Phys. A*, **204**, 465 (1973).
(39) J. R. Nix and A. J. Sierk, Los Alamos Preprint, LA-UR-75-1643 (1975).
(40) J. Wilczyński, *Nucl. Phys. A*, **216**, 386 (1973).
(41) R. Bass, *Nucl. Phys. A*, **231**, 45 (1974).
(42) J. Wilczyński, *Phys. Lett. B*, **47**, 484 (1973).

Table I
Comparison of Parameters Deduced from the Optical and Fresnel Models for a ^{209}Bi Target and Several Heavy-Ion Projectiles[19,28]

				Optical			Fresnel		
Projectile	Energy, MeV	η	$\theta_{1/4}^{cm}$, deg	$l_{1/2}$	R_{SA}, fm	σ_R, mbarn	l_{max}	R_{INT}, fm	σ_R, mbarn
^{40}Ar	340	80.63	47	186	13.30	2480	185	13.21	2382
	286	87.91	60	150	13.35	1926	151	13.43	1887
^{84}Kr	712	161.6	50.5	346	14.25	2606	343	14.16	2533
	600	175.9	66	272	14.28	1922	270	14.24	1880
^{136}Xe	1130	244.8	54	484	15.21	2780	481	15.10	2700

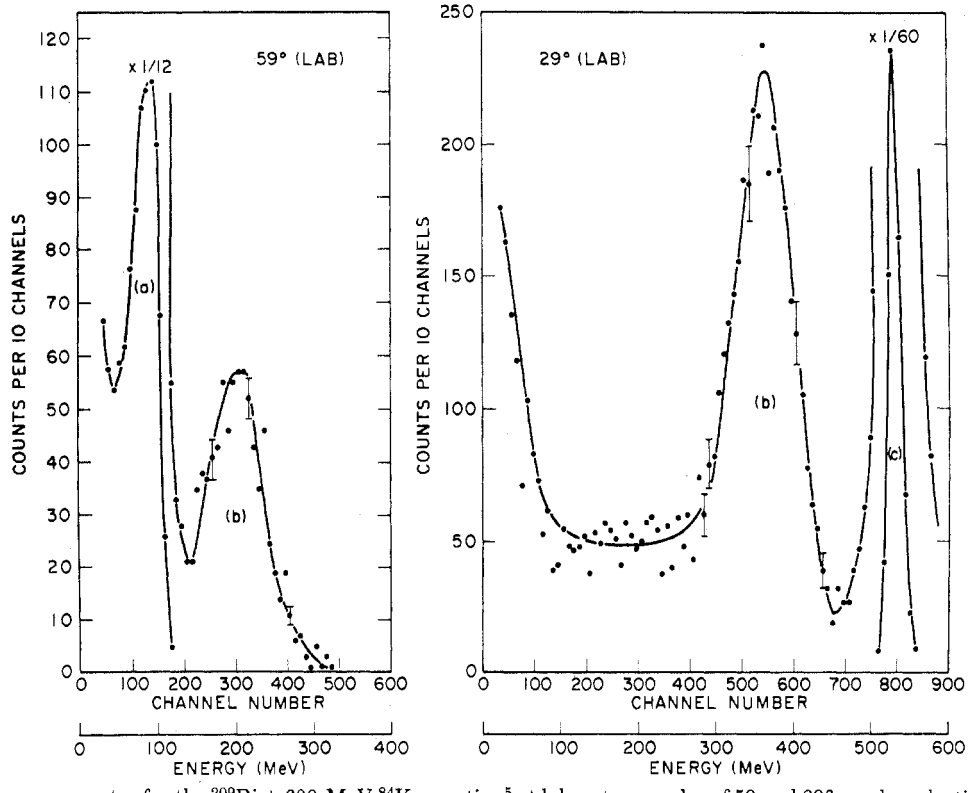

Figure 5. Singles energy spectra for the ^{209}Bi + 600-MeV ^{84}Kr reaction[5] at laboratory angles of 59 and 29°: peak a, elastic ^{209}Bi recoils; peak b, light-mass fragment from strongly damped collisions; peak c, elastic ^{84}Kr events.

kinetic-energy spectrum at a fixed angle contains two energy groups, the higher and lower energy groups presumably due to different angular momenta being emitted at positive and negative angles, respectively. Similar behavior has since been reported for other reactions[21,43] and shown not to be due to fission. The deflection angle of the reaction products depends upon a delicate balance between the attractive and repulsive forces which determine the penetration depth of the trajectory.

Damping of the Kinetic Energy into Internal Excitation Energy. A characteristic feature of energy spectra measured for very heavy ion reactions is the presence of a peak which is well removed and reduced in energy from the elastic peak. This peak is usually easily resolved at all angles, except in an angular range of several degrees around $\theta_{1/4}$ where grazing collisions are important. Examples of the single-counter energy spectra from our first ^{84}Kr experiments in 1973 for the ^{209}Bi + ^{84}Kr (600 MeV) reaction[5] are shown in Figure 5 where the uncorrected apparent energies are plotted. At 59°(lab) the lower energy peak, a, is the elastic ^{209}Bi recoil peak and peak b is the lighter mass fragment from the strongly damped collision process. At 29°(lab), peak b is again the light mass fragment from the strongly damped collisions and peak c is the elastic ^{84}Kr peak. Coincidence measurements have shown that peak b in each spectrum is due to the lighter mass fragment from a binary process where the average masses of the two groups are near those of the target and projectile.

Of great interest is the total kinetic energy (TKE) release for this new process. Although a few coincidence measurements have been made, most estimates of the TKE are based on singles measurements and the assumption of a two-body reaction process. Aside from the experimental corrections, there is an additional uncertainty in the TKE values due to the assumptions made in the correction for particle emission during deexcitation of the primary products of the strongly damped collisions. In spite of these difficulties, the qualitative results from several heavy-ion experiments is that large cross sections are observed for reaction products with kinetic energies which are equal or nearly equal to the Coulomb energy of the two product nuclei. In a number of cases the TKE values extend to values well below the calculated Coulomb energies of spherical

(43) K. L. Wolf, J. R. Huizenga, J. R. Birkelund, H. Freiesleben, and V. E. Viola, *Bull. Am. Phys. Soc.*, **21**, 31 (1976).

Table II
Centroid and fwhm of the Charge Distribution of the Xe-like Fragment for Various Energy Bins[a]

Bin	E_{Lab}, MeV	TKE, MeV	$d\sigma/d\Omega$, mbarn/sr	$\langle Z \rangle$	fwhm$_Z$
1	946	684		54	3.3 ± 0.2
2	926	662	1410	54.1 ± 0.1	4.0 ± 0.2
3	896	640	1095	54.0 ± 0.1	4.6 ± 0.2
4	857	605	700	54.8 ± 0.1	4.5 ± 0.2
5	818	575	553	54.8 ± 0.2	5.4 ± 0.2
6	779	540	515	54.8 ± 0.2	6.3 ± 0.2
7	740	510	471	55.1 ± 0.2	7.8 ± 0.3
8	700	475	405	55.0 ± 0.2	8.3 ± 0.2
9	661	442	313	55.1 ± 0.2	11.1 ± 0.3
10	622	410	234	55.4 ± 0.3	14.3 ± 0.5
11	583	375	160	57.1 ± 0.5	16.8 ± 1.0

[a] Measured at a laboratory angle of 29.8° for the $^{209}Bi + ^{136}Xe$ reaction at 1130 MeV (laboratory energy).[19] Both energies are given to the middle of the bin and the TKE (total kinetic energy) values are corrected for neutron emission.

products and give direct evidence for nuclear distortion of the fragments at separation. The degree of fragment deformation at separation is difficult to ascertain since part of the observed TKE is rotational energy and, depending on the strength of the nuclear viscosity, some fraction of the observed TKE is in fragment translational energy. One concludes from these results that touching collisions between complex nuclei have a high probability to form a relaxed system where, during the short interaction time, considerable damping of the initial energy of relative motion occurs, giving two fragments with large internal excitation energies.

The degree of energy damping varies with angle, especially for angles near $\theta_{1/4}$ where large contributions of "grazing collisions" occur. However, there appear to be some events which are fully damped at all angles, and the TKE of these fully damped events are approximately independent of bombarding energy. Comparisons of the TKE values at two bombarding energies are difficult to interpret due to different average collective energies introduced by the two angular-momentum distributions. This same difficulty arises for comparisons of TKE values for two angles at the same bombarding energy due to possible angular momentum fractionation.

Nucleon Transfer and Reaction Product Masses. Information about the nucleon transfer associated with this new reaction process has been obtained by several experimental techniques. These methods include (1) coincidence measurements of the energies of each fragment,[4,5] (2) counter telescope measurements of the charge distributions of the lighter mass fragment,[7,14,15,17-20] (3) time-of-flight mass determinations,[8,21] and (4) radiochemical mass measurements.[6,44] The more detailed results on the reaction product masses come from the experimental techniques where both fragments are studied simultaneously. However, based on limited coincidence experiments, the strongly damped reaction is a binary process (for heavy targets, one of the fragments may sequentially fission). Hence, detailed studies of one of the final fragments are very instructive (it is usually easier to study the lighter fragment).

One of the important general results from the above mass measurements is that the reaction product masses from this new process are distributed into two groups, with average masses near those of the target and the projectile. Such a mass distribution is in sharp contrast to the symmetric mass distribution predicted from a high-energy fusion–fission reaction mechanism. The above type of experiments have also shown that considerable nucleon transfer takes place during the lifetime of the strongly damped collisions. The distribution of the charges and masses of the reaction products is correlated with the kinetic energy dissipated. This is illustrated in Figure 6 for the $^{209}Bi + ^{136}Xe$ (1130 MeV) reaction. These results were obtained with a ΔE–E counter telescope system composed of a thin 8-μm silicon transmission detector and a thick stopping detector.

The charge distributions of the Xe-like fragment as a function of kinetic energy (see Table II for identification of the energy bins), measured at the peak of the angular distribution $\theta_{lab} = 29.8°$, are shown in Figure 6. The solid curves of Figure 6 are Gaussian fits to the charge distribution data. The parameters of the Gaussians, $\langle Z \rangle$ and fwhm, are listed in Table II for each curve. Energy bin 1 corresponds to elastic scattering and illustrates the Z resolution of the telescope. This contribution to the width must be subtracted from the data in Table II. The kinetic-energy spectrum at 29.8° contains events of all degrees of energy damping, as shown by the cross section data in Table II. As displayed in Figure 6, the charge distribution broadens as more kinetic energy is lost in the collision. Although the width of the charge distribution broadens with energy damping, the centroid of the distribution stays fixed to within a few units of Xe. The charge distributions at angles forward and backward of 29.8° have similar shapes to those of Figure 6, and differ only in that the highly damped energy bins with large values of the fwhm comprise the major fraction of the cross section at these angles.

The average amount of mass transfer is correlated with the potential energy of the two-nucleus or binary-intermediate system. The direction of mass transfer for very heavy ion reactions is to increase the mass of the lighter fragment at the expense of the heavy fragment, in agreement with potential energy arguments. The magnitude of the mass transfer to the projectile is larger for the $^{209}Bi + ^{84}Kr$ reaction than for the $^{209}Bi + ^{136}Xe$ reaction, a result which correlates with the greater driving force. In our view, the so-called "gold-

(44) N. T. Anh, Yu. Ts. Oganessyan, and Yu. E. Penionzhkevich, Proceedings of the Conference on Reactions between Complex Nuclei, Nashville, Tenn., 1974; Tu. Ts. Organessian, and Y. E. Penionzhkevich, Dubna Preprint E7-9187 (1975).

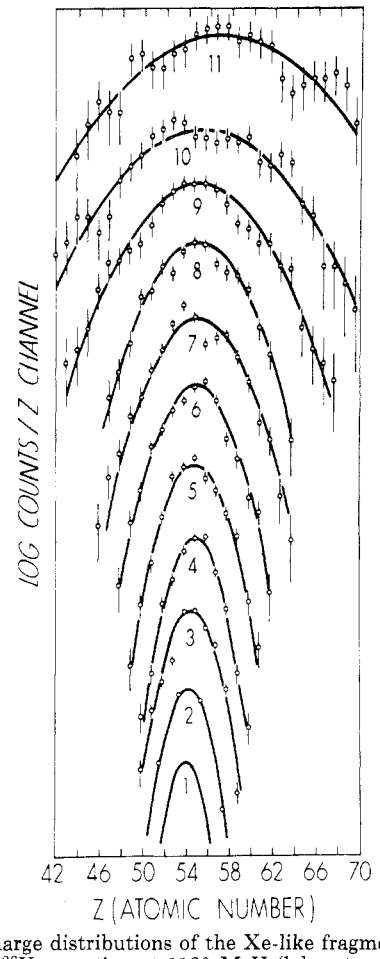

Figure 6. Charge distributions of the Xe-like fragment formed in the $^{209}Bi + {}^{136}Xe$ reaction at 1130 MeV (laboratory energy) as a function of the fragment kinetic energy.[19] The fragment kinetic energy decreases as the bin number increases (details in Table II).

finger peak" with $A \approx 200$ observed in radiochemical mass measurements[6] for the $^{238}U + {}^{84}Kr$ reaction is a remnant of the heavy-mass fragment in the strongly damped collision process. On the basis of the theoretical driving force, one expects considerable mass transfer away from the heavy fragment in this reaction. However, most of the primary excited heavy products sequentially fission except for those fragments with masses in the vicinity of the lead region, which are formed by massive nucleon transfer.

Theories of Strongly Damped Collisions

Several authors have described heavy-ion reactions in terms of a classical scattering of two spherical nuclei with conservative and dissipative forces.[45-51] In such a classical dynamical model the internal degrees of freedom corresponding to rotation of the ions are included along with the center-of-mass coordinates. The conservative forces include the repulsive Coulomb and attractive nuclear forces. The phenomenological dissipative forces are introduced to couple the relative motion to intrinsic degrees of freedom and allow for energy and angular-momentum transfer.

Such a Lagrangian approach has yielded results which are in qualitative agreement with the experimental results on strongly damped collisions. However, such simple models must be modified to include mass transfer[50] and deformation effects[51,52] which are important features of the strongly damped process. Although these classical macroscopic models with friction give one important insights into heavy-ion reactions, a microscopic description of nuclear energy dissipation is required, and several articles on this subject have already appeared.[53]

Nonequilibrium quantum-statistical mechanics has also been applied to the strongly damped collisions[54,55] which represent equilibration processes of rather small quantal systems which are initially far from equilibrium. This model assumes (1) that the nuclei lose a large fraction of their relative kinetic energy into internal excitation energy and form a binary nuclear complex which rotates and decays into two deformed fragments; (2) a diffusion process occurs during the lifetime of the intermediate complex and leads to exchange of nucleons between the two touching fragments; and (3) a large number of degrees of freedom are involved and transitions between different channels are determined by the master equation approach to describe the time-dependent structure of the system.

From the Fokker–Planck equation, one relates the fwhm of the charge distribution to the charge diffusion coefficient D_Z and interaction lifetime t by $(\text{fwhm})^2 = (16 \ln 2) D_Z t$.[54] If D_Z is assumed constant, the average lifetime of bins 10 and 11 in Table II is approximately 30 times longer than the average lifetime of bins 2 to 4. If the latter lifetime is assumed to be 10^{-22} s, $D_Z = (\frac{3}{4}) \times 10^{22}$ (charge units)^2 s^{-1}, a value in good agreement with a similar estimate from the $^{232}Th + {}^{40}Ar$ reaction.[54] With this value of D_Z, the lifetimes of bins 5 to 11 vary from 0.2 to 3.3×10^{-21} s. These lifetimes are in the range of those determined from the angular velocities of binary systems formed in the $^{209}Bi + {}^{84}Kr$ reaction.[52]

A number of more precise measurements of the properties of strongly damped collisions are essential to test various aspects of the theory. Of special importance are experiments which distinguish energy dissipation by one-body and two-body viscosities.[22] It has already been shown that a high two-body viscosity is inconsistent with experimental fission fragment kinetic energies.[56] Are strongly damped heavy ion collisions and fission both explainable in terms of a high one-body nuclear viscosity? The excitation energy and angular momentum of each fragment in the strongly damped collision, as well as the degree to which equilibrium is attained in each fragment, also need to be measured. The latter question can be investigated by a careful study of the energy distribution of light particles emitted during the deexcitation of the primary fragments.

The fact that the new strongly damped collision process is so dominant for reactions between complex

(45) W. J. Swiatecki and S. Bjornholm, *Phys. Rep.* **4c**, 326 (1972).
(46) C. F. Tsang, *Phys. Scr.*, **10A**, 90 (1974).
(47) J. P. Bondorf, D. Sperber, and M. I. Sobel, *Phys. Rep.* **15c**, 83 (1974).
(48) D. H. E. Gross and H. Kalinowski, *Phys. Lett. B*, **48**, 302 (1974).
(49) R. A. Broglia, C. H. Dasso, and Aa. Winther, *Phys. Lett. B*, **53**, 301 (1974).
(50) D. H. E. Gross, H. Kalinowski, and J. N. De, *Lect. Notes, Phys. (Heidelberg)*, **33**, 194 (1975).
(51) H. H. Deubler and K. Dietrich, *Phys. Lett. B*, **56**, 241 (1975).
(52) J. P. Bondorf, J. R. Huizenga, M. I. Sobel, and D. Sperber, *Phys. Rev. [Sect.] C*, **11**, 1265 (1975).
(53) S. E. Koonin and J. R. Nix, *Phys. Rev. [Sect.] C*, **13**, 209 (1976), and references therein.
(54) W. Nörenberg, *Phys. Lett. B*, **52**, 289 (1975); *Z. Phys. A*, **274**, 241 (1975).
(55) L. G. Moretto and J. S. Sventek, *Phys. Lett. B*, **58**, 26 (1975); L. G. Moretto, R. P. Babinet, J. Galin, and S. G. Thompson, *ibid.*, **58**, 31 (1975).
(56) J. R. Nix and A. J. Sierk, *Phys. Scr.*, **10A**, 94 (1974).

nuclei makes the production of superheavy elements by those reactions very unlikely insofar that the net mass transfer goes from the heavy to the light fragment. However, massive nucleon transfer to the heavy fragment to produce a superheavy element in the tail of the heavy fragment mass distribution is possible with a very small cross section (<0.1 nbarn). At this time the production of superheavy elements seems most likely with a very asymmetric combination of target and projectile, e.g., ^{48}Ca plus a very heavy target.

Many thanks are due my collaborators in these heavy-ion experiments, J. R. Birkelund, H. Freiesleben, W. U. Schröder, K. L. Wolf, J. P. Unik, and V. E. Viola. Support from the U.S. Energy Research and Development Administration is gratefully acknowledged.

The Structure of Adsorbed Gas Monolayers

Jeffrey C. Buchholz and Gabor A. Somorjai*

Materials and Molecular Research Division, Lawrence Berkeley Laboratory and Department of Chemistry, University of California, Berkeley, California 94720

Received December 1, 1975

One of the most exciting observations of low-energy electron diffraction (LEED) studies of adsorbed monolayers on low Miller index crystal surfaces is the predominance of ordering within these layers. These studies have demonstrated the existence of a large number of surface structures formed upon adsorption of a large number of atoms and molecules on a variety of solid surfaces. Conditions range from low-temperature inert gas physisorption to chemisorption of reactive gases and hydrocarbons at room temperature and above. A listing of over 200 adsorbed surface structures, mostly of small molecules adsorbed on low Miller index surfaces, can be found in a recent review.[1] Not only is there ordering of the adsorbed atoms and molecules, but the surface structures formed are different from crystal face to crystal face.

Studies of the ordered surface structures of adsorbates yield information about the bonding geometry for adsorbed molecules and thus detailed information about the interaction between the adsorbed molecule and the substrate and the interactions between adsorbed molecules. In view of the results of the LEED studies which show markedly different adsorption structures for the same gas adsorbed on different crystal faces of a material, the chemical bonding between the adsorbate and the surface of the solid appears to vary markedly with the type of surface site, i.e., atomic geometry. A detailed understanding of the structure is thus necessary before surface phenomena involving adsorption and catalyzed surface reactions can be understood on a molecular level. Simpler models of a surface which neglect the details of the structure of solid surfaces, considering the surface to consist of noninteracting adsorption sites, cannot account for the large number of surface structures observed that have a periodicity different from that of the substrate.

For surface reactions, some of the atomic sites with a smaller number of nearest neighbors (atomic steps, kinks, etc.) are primarily responsible for breaking chemical bonds of large binding energy (H–H, C–H, C–C, etc).[2] Identification and tailoring of the active sites of low coordination number to perform selective bond scissions is one of the exciting new areas of surface chemistry.

During catalytic reactions, the surface, including adsorbed monolayers, sometimes appears to act as a template for the reaction in a manner analogous to the action of enzymes in biological catalysis. For example, the conversion of *n*-heptane to toluene on a platinum surface proceeds only in the presence of an ordered carbonaceous layer on the substrate.[2] A disordered layer does not catalyze the reaction. The exploration and utilization of this template effect of adsorbed monolayers in catalysis is another exciting area in the study of adsorbed layers.

In this Account we review some of the recent work aimed at understanding the structure of adsorbed monolayers and its role in determining the chemical reactivity of a surface. First we will discuss the phenomenon of ordered adsorption with the object of determining what the study of the structure of adsorbed monolayers tells us about the basic interactions at a surface, that is, the type and strength of adsorbate–substrate and adsorbate–adsorbate chemical bonds. Second, we will discuss studies of adsorbed monolayer structures important to reactions at a surface. These include reactions of the adsorbed molecules with the substrate to form new surface phases such as oxides and adsorption of two components simultaneously in which a new surface structure is formed due to interaction between these species. Third, we will discuss work related to the effect

Gabor A. Somorjai is Professor of Chemistry at University of California, Berkeley, and Principal Investigator in the Molecular Materials Research Division at Lawrence Berkeley Laboratory. He was born in Budapest, and studied at the University of Technical Sciences there for his B.S. degree. After moving to the United States, he earned the Ph.D. at Berkeley in 1960, and then joined the research staff at IBM, Yorktown Heights, N.Y. He returned to Berkeley in 1964. His principal research interests are in the field of surface science.

Jeffrey C. Buchholz received his B.S. degree at the University of Wisconsin—Eau Claire, and his Ph.D. (in 1974) at University of Wisconsin—Madison. He is doing postdoctoral research with Dr. Somorjai at Berkeley.

(1) G. A. Somorjai and L. L. Kesmodel, *MTP Int. Rev. Sci.: Phys. Chem., Ser. Two*, 7 (1975).

(2) B. Lang, R. W. Joyner, and G. A. Somorjai, *Proc. Roy. Soc. London, Ser. A*, 331, 335 (1972).